ACS ORGANIC & INORGANIC Au
AN OPEN ACCESS JOURNAL OF THE AMERICAN CHEMICAL SOCIETY

pubs.acs.org/orginorgau

Article

Reactivity of [(PNP)Mn(CO)$_2$] with Organophosphates

Brooke N. Livesay, Jurgen G. Schmidt, Robert F. Williams, Brennan S. Billow,* and Aaron M. Tondreau*

Cite This: *ACS Org. Inorg. Au* 2023, 3, 199−208

Read Online

ACCESS | Metrics & More | Article Recommendations | Supporting Information

ABSTRACT: Organophosphorus nerve agents (OPAs) are a toxic class of synthetic compounds that cause adverse effects with many biological systems. Development of methods for environmental remediation and passivation has been ongoing for years. However, little progress has been made in therapeutic development for exposure victims. Given the postexposure behavior of OPA materials in enzymes such as acetylcholinesterase (AChE), development of electrophilic compounds as therapeutics may be more beneficial than the currently employed nucleophilic countermeasures. In this report, we present our studies with an electrophilic, 16-electron manganese complex (^{iPr}PNP)Mn(CO)$_2$ (**1**) and the nucleophilic hydroxide derivative (^{iPr}PN^{H}P)Mn(CO)$_2$(OH) (**2**). The reactivity of **1** with phosphorus acids and the reactivity of **2** with the P−F bond of diisopropylfluorophosphate (DIPF) were studied. The role of water in both nucleophilic and electrophilic reactivity was investigated with the use of ^{17}O-labeled water. Promising results arising from reactions of both **1** and **2** with organophosphorus substrates are reported.

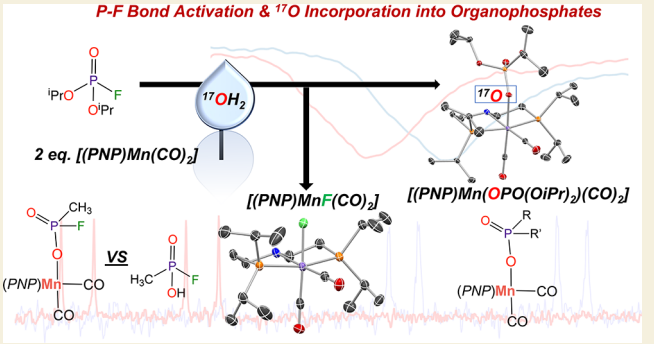

KEYWORDS: *PNP, manganese, organophosphate, methyl(fluoro)phosphonate, ambiphilic*

INTRODUCTION

Organophosphorus nerve agents (OPAs) represent a highly toxic class of compounds employed as chemical warfare agents (CWAs). OPAs remain one of the most abused weapons of fear, which provides an imperative to investigate their fundamental chemical behavior. Their use in Russia, England, Malaysia, and Syria, and more recent attribution as the origin of Gulf War syndrome, highlight the continued exploitation of OPAs as weapons of terror, assassination, and area denial.[1] Recent literature reports on the interaction between OPAs and molecular transition-metal systems have lagged[2−5] behind those of metal−organic framework (MOF)-based systems.[6−22] While proven methods exist for effective large-scale agent destruction and surface decontamination,[23−35] the current in vivo therapeutic method is decades-old and consists of a cocktail of oximes and atropine administered near their toxicity limits. The oximes act as a nucleophile to the OPA,[36] yet their effectiveness is severely limited due to the nature of action of OPAs in the body following exposure.

The primary biological mode of action of an OPA occurs via bonding to an −OH group of a serine residue of acetylcholinesterase (AChE).[37] Inhibition is achieved by binding to the active site of the enzyme and blocking the uptake and hydrolysis of acetylcholine, which results in muscle paralysis leading to suffocation. Subsequent hydrolysis of the serine-bound OPA in the active site of AChE results in an "aged" adduct (Figure 1, top).[38−40] In the "aging" process, the OPA alkoxide side chain is converted to an anionic oxygen at

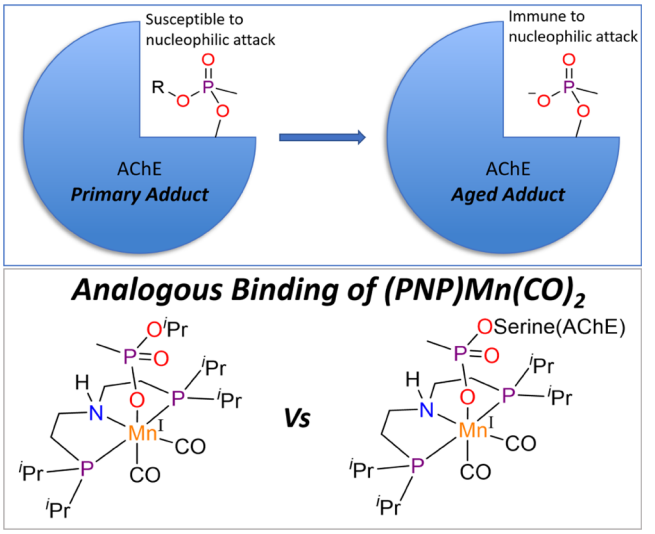

Figure 1. (Top) Graphical representation of the aging process of an enzyme-bound OPA, such as sarin (GB). (Bottom) Comparison of (^{iPr}PN^{H}P)Mn(CO)$_2$ binding to a small-molecule phosphonate and to an aged, AChE-bound sarin molecule.

Received: February 3, 2023
Revised: April 20, 2023
Accepted: April 24, 2023
Published: May 25, 2023

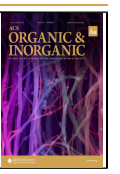

physiological pH, and nucleophilic oxime therapy is rendered ineffective. Consequently, the treatment for nerve agent exposure must begin promptly to avoid "aging" of the OPA in the active site of the enzyme. Only recently have electrophilic molecules been investigated to reactivate aged OPA−enzyme complexes.[41,42] Development of an ambiphilic therapeutic that can target both the primary adduct and the "aged" OPA adduct could facilitate the hydrolysis of the serine−phosphorus bond, reactivating the enzyme at any time after exposure (Figure 1, bottom).

Prior work using (^{iPr}PNP)Mn(CO)$_2$ (**1**, ^{iPr}PNP = N-(CH$_2$CH$_2$(^{iPr2}P))$_2$), a low-spin 16-electron manganese(I) complex, has demonstrated wide utility, including ambiphilic reactivity. Catalytic reactions concerning the generation[43−48] or consumption[49−53] of H$_2$ using **1** have been well studied, and the ability to tailor the reactivity of **1** by altering reaction conditions is a valuable property. The electrophilic reactivity of **1** has been demonstrated with several element−hydrogen bonds, including carboxylic acid substrates that are isolobal and isoelectronic with OPA surrogate substrates.[54] Additionally, a reversible equilibrium of 1,2-addition and 1,2-elimination of water (H$_2$O) can be used to isolate a nucleophilic Mn−OH complex, (^{iPr}PN^{H}P)Mn(CO)$_2$(OH) (**2**).[55] The hydroxide moiety in **2** retains its nucleophilic character due to the low-spin 3d^6 electronic configuration of the Mn center and related filled π orbitals, a property previously demonstrated through reactivity.[55] Aldehyde addition to **2** generated the corresponding Mn-bound carboxylate with concomitant formation of H$_2$ in an aldehyde−water shift reaction,[55] while nitriles were cleanly converted to their corresponding organic carboxamide via hydration reactivity mediated by **2**.[56] Employing this bimodal reactivity with organophosphate substrates allows the exploration of OPA surrogates with Mn acting as either a nucleophile or an electrophile.

The results from an investigation into the reactivity of **1** and **2** with organophosphate substrates are described. Electrophilic reactions of **1** with P(O)O−H and P(O)O$^-$ groups were performed. Alternatively, the nucleophilic hydroxide of **2** was studied to facilitate the cleavage of P−F bonds. Due to the formation of H−F during P−F bond hydrolysis, observation of Mn−F species is also expected, consequently an independent synthesis of the expected Mn−F species was performed. The reactivity of **1** and **2** with established precursors and surrogates of organophosphorus-based CWAs was explored and the resultant products are isolated and characterized. Additional studies using ^{17}O-labeled water provide insight into the mode of action of **1** and **2** with OPA substrates.

EXPERIMENTAL SECTION

Caution! Organofluorophosphates are toxic and release HF upon hydrolysis. All work with these materials should be performed in a well-ventilated fume hood or drybox by persons experienced with their handling. Materials should be passivated using solutions of bleach and/or aqueous base (e.g., 1 M NaOH).

All air- and moisture-sensitive manipulations were carried out using standard Schlenk techniques or in a Vac Atmospheres drybox containing a purified argon atmosphere. THF, benzene, toluene, diethyl ether, and *n*-hexane were dried on molecular sieves and shaved sodium before use. THF-d_8 and C$_6$D$_6$ were purchased from Millipore Sigma and dried over 4 Å molecular sieves. The chemicals KHMDS, NaHMDS, diisopropylfluorophosphate, dimethylphosphate, and diisopropylphosphate were ordered from Millipore Sigma and were used after degassing. The complexes (^{iPr}PN^{H}P)Mn(CO)$_2$Br,[57] (^{iPr}PN^{H}P)Mn(CO)$_2$[55] (**1**), (^{iPr}PN^{H}P)Mn(OH)(CO)$_2$[55] (**2**), and monofluor[58] were prepared as previously described. (^{iPr}PN^{H}P)Mn-(^{17}OH)(CO)$_2$ (**^{17}O-2**) was prepared analogously to **2** using ^{17}OH$_2$.

^{1}H NMR, ^{13}C NMR, ^{19}F NMR, and ^{31}P NMR spectra were recorded on a Bruker Avance 400 MHz spectrometer operating at 400.132, 100.627, 376.498, and 161.978 MHz, respectively. All ^{1}H and ^{13}C{^{1}H} NMR chemical shifts are reported relative to SiMe$_4$ using the ^{1}H (residual in the deuterated solvents) and ^{13}C{^{1}H} chemical shifts of the solvent as a secondary standard. Multiplicity, integration, and coupling constants (Hz) are provided when appropriate. The NMR splitting patterns are abbreviated as follows: s, singlet; br s, broad singlet; d, doublet; dd, doublet of doublets; ddd, doublet of doublets of doublets; t, triplet; br t, broad triplet; q, quartet; dq, doublet of quartets; h, heptet; and m, multiplet. Infrared spectra were collected on a Thermo Scientific Nicolet iS10 spectrometer equipped with an ATR measurement attachment.

Single crystals suitable for X-ray diffraction were coated with N-paratone (dried under reduced pressure overnight at 100 °C) or Krytox oil in a drybox, placed on a nylon loop, and then transferred to the goniometer head of a Bruker X8 APEX 2 (for complex **2**) diffractometer equipped with a molybdenum X-ray tube (λ = 0.71073 Å), a Bruker D8 Quest (for complexes **5** and **3**) equipped with a molybdenum X-ray tube (λ = 0.71073 Å), a Bruker D8 Quest diffractometer configured with a CPAD Photon II area detector and a molybdenum (λ = 0.71073 Å) IμS 3.0 micro source, or a Rigaku XtaLAB mini II equipped with a HyPix-Bantam detector and a molybdenum X-ray tube (λ = 0.71073 Å) for the complexes collected at room temperature (**^{17}O-4** and **8**). A hemisphere routine was used for data collection and determination of lattice constants. Crystals were cooled using an oxford cryostream cooling to 100 K or collected at room temperature (Rigaku XtaLAB mini II). Space groups were identified, and the data were processed using the Bruker SAINT+ program and corrected for absorption using the SADABS.[59] The structures were solved using intrinsic phasing (SHELXT)[60] completed by subsequent Fourier synthesis and refined by full-matrix least-squares procedures.[61,62] Olex2 software was used to perform data workup.[63]

Synthesis of (^{iPr}PN^{H}P)Mn(CO)$_2$F, 3

(^{iPr}PN^{H}P)Mn(CO)$_2$Br (0.050 g, 0.1 mmol) was dissolved in ∼5 mL of THF and loaded into a 20 mL scintillation vial along with a magnetic stir bar. Silver fluoride, AgF, (0.013 g, 0.1 mmol) was added as a solid to the vial. The vial was then capped and covered with aluminum foil. The solution was left to stir vigorously for 24 h. After, the volatiles were removed under reduced pressure, and the remaining solids were extracted with toluene and filtered over a glass fiber filter. The filtrate was then dried to a constant mass, and the yellow residue was dissolved in a minimal amount of diethyl ether. The ether solution was then placed in a −35° freezer overnight, yielding diffraction quality pale yellow crystals of **3** (0.027 g, 62%). Note: incomplete halide exchange was observed, affecting bulk analysis; please see the provided NMR spectra. Anal. calcd for C$_{18}$H$_{37}$FMnNO$_2$P$_2$: C, 49.66; H, 8.57; N, 3.22. Found: C, 48.22; H, 8.49; N, 3.12. ^{1}H NMR (C$_6$D$_6$, 20 °C): δ 2.56 (m, 4H), 2.31 (s, 2H), 2.07 (m, 2H), 1.62 (s, 2H), 1.52 (s, 6H), 1.33 (dd, J = 6.9 Hz, 6H), 1.24 (d, J = 6.9 Hz, 6H), 1.12 (s, 7H). ^{31}P{^{1}H} NMR (C$_6$D$_6$, 20 °C): δ 89.16. ^{19}F NMR (C$_6$D$_6$, 20 °C): δ −378.63. ^{13}C{^{1}H} NMR (C$_6$D$_6$, 20 °C): δ 232.3, 228.1, 52.3, 26.5, 25.0 (t), 24.6 (br t), 20.9, 20.1, 19.1, 18.2.

Synthesis of (^{iPr}PN^{H}P)Mn(CO)$_2$(OPO(^{i}Pr)$_2$), 4

(^{iPr}PNP)Mn(CO)$_2$ (0.040 g, 0.096 mmol) was dissolved in ∼2 mL of THF and loaded into a 20 mL scintillation vial along with a magnetic stir bar. To this solution, diisopropylphosphate, (^{i}PrO)$_2$OP(OH), DIP, (0.018 g, 0.10 mmol) was added. Next, a 20% THF solution of H$_2$O (0.002 g H$_2$O, 0.010 g solution, 0.11 mmol) was added. A color change of the solution was noted after ∼3 h to a pale orange from the initial red color. The reaction was allowed to stir for ∼16 h, and the color had changed to yellow. The solution was then concentrated. The resulting solid was dissolved in benzene, filtered, and left to sit undisturbed at room temperature, yielding diffraction quality yellow

https://doi.org/10.1021/acsorginorgau.3c00003
ACS Org. Inorg. Au 2023, 3, 199−208

Scheme 1. Proposed Products from the Reaction between 2 and OPA; P−F Bond Hydrolysis Yields the Expected Mn−Phosphate (a) and Generates HF Which Yields 3 (b)

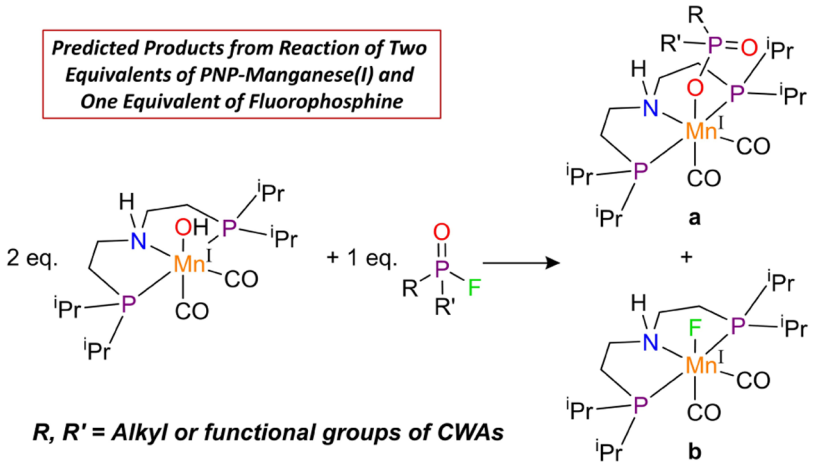

crystals of **4** (0.029 g, 51%). Anal. calcd for $C_{24}H_{51}MnNO_6P_3$: C, 48.24; H, 8.60; N, 2.34. Found: C, 48.07; H, 8.37; N, 2.32. ^{1}H NMR (C_6D_6, 20 °C): δ 5.43 (t, 1H, N−H), 4.45 (dd, J = 6.2 Hz, 2H), 3.03 (m, 2H), 2.91 (m, 2H), 2.29−2.12 (m, 4H), 2.03 (m, 2H), 1.81 (m, 2H), 1.57 (dd, J = 7.5 Hz, 6H), 1.39 (dd, J = 7.1 Hz, 6H), 1.29−1.15 (m, 18H), 1.08 (dd, J = 3.7 Hz, 6H). ^{31}P{^{1}H} NMR (C_6D_6, 20 °C): δ 84.18, 4.57. ^{13}C{^{1}H} NMR (C_6D_6, 20 °C): δ 231.5, 229.8, 68.6, 52.9, 30.2, 27.0, 25.3 (t), 24.4 (br t), 24.3 (t), 20.7, 20.6, 19.1, 17.7.

Synthesis of (^{iPr}PN^{H}P)Mn(CO)$_2$(OPO(OMe)$_2$), 5

(^{iPr}PNP)Mn(CO)$_2$ (0.040 g, 0.096 mmol) was dissolved in ∼2 mL of THF and loaded into a 20 mL scintillation vial along with a magnetic stir bar. To this stirring solution, an equivalent of dimethylphosphate, DMP, (MeO)$_2$OP(OH), (0.012 mg, 0.10 mmol) was added. There was a noticeable color change of the solution from red to yellow upon addition of the phosphate. The solution was allowed to stir for ∼1 h, at which time it was then concentrated, filtered, and left to sit undisturbed at room temperature, yielding X-ray diffraction quality large pale yellow crystals of **5** (0.035 g, 67%). Note: Combustion analysis was low in carbon; please see the provided NMR spectra as an additional measure of bulk purity. Anal. calcd for $C_{20}H_{43}MnNO_6P_3$: C, 44.37; H, 8.01; N, 2.59. Found: C, 43.90; H, 8.17; N, 2.55. ^{1}H NMR (C_6D_6, 20 °C): δ 5.87 (br s, 1H), 3.43 (br s, 6H), 2.88 (br s, 4H), 2.21 (br s, 4H), 1.83 (br s, 4H), 1.56 (br s, 6H), 1.36 (br s, 6H), 1.23 (br s, 6H), 1.09 (br s, 6H). ^{31}P{^{1}H} NMR (C_6D_6, 20 °C): δ 84.30, 9.30. ^{13}C{^{1}H} NMR (C_6D_6, 20 °C): δ 231.8, 229.9, 52.8, 27.4, 26.0, 24.3 (t), 20.7, 20.5, 19.0, 17.9.

Synthesis of (^{iPr}PN^{H}P)Mn(CO)$_2$(OP(O)Me(O^{i}Pr)), 6

(^{iPr}PNP)Mn(CO)$_2$ (0.100 g, 0.240 mmol) was added to a 20 mL scintillation vial along with a magnetic stir bar and was then dissolved in ∼2 mL of *n*-hexane. To this stirring solution, a 10% solution of isopropyl methylphosphonate, MeP(O)(O^{i}Pr)(OH), MIP, (0.033 g, 0.241 mmol) in THF was added dropwise that induced a color change of the reaction solution from red to yellow. The clear reaction solution was cooled to −30 °C, yielding X-ray diffraction quality crystals. The yellow crystalline material was isolated via filtration and held under reduced pressure to a constant mass. Analysis of the material confirmed formation of **6** (0.122 g, 93%). Note: Combustion analysis was low in carbon; please see the provided NMR spectra as an additional measure of bulk purity. Anal. calcd for $C_{22}H_{47}MnNO_5P_3$: C, 47.74; H, 8.56; N, 2.53. Found: C, 47.09; H, 8.50; N, 2.30. ^{1}H NMR (C_6D_6, 20 °C): δ 6.09 (t, J = 11.4 Hz, 1H, N−H), 4.33 (h, J = 6.1 Hz, 1H), 3.27 (h, J = 7.0 Hz, 1H), 3.06−2.79 (m, 2H), 2.67 (h, J = 7.2 Hz, 1H), 2.20 (m, 5H), 2.00−1.72 (m, 3H), 1.63−1.46 (m, 6H), 1.45−1.32 (m, 6H), 1.25 (m, 12H), 1.07 (m, 9H). ^{31}P{^{1}H} NMR (C_6D_6, 20 °C): δ 84.53, 31.79. ^{13}C{^{1}H} NMR (C_6D_6, 20 °C): δ 6.1 (t, J = 11.4 Hz, 1H, N−H), 4.3 (h, J = 6.1 Hz, 1H), 3.3 (h, J = 7.0 Hz, 1H), 3.1−2.8 (m, 2H), 2.7 (h, J = 7.2 Hz, 1H), 2.2 (m, 5H), 2.0−1.7 (m, 3H), 1.6−1.5 (m, 6H), 1.5−1.3 (m, 6H), 1.3 (m, 12H), 1.1 (m, 9H).

Synthesis of (^{iPr}PN^{H}P)Mn(CO)$_2$(OP(O)MeF), 7

(^{iPr}PNP)Mn(CO)$_2$ (0.100 g, 0.240 mmol) was added to a 20 mL scintillation vial along with a magnetic stir bar and was then dissolved in ∼2 mL of *n*-hexane. To this stirring solution, a 10% solution of fluoro methylphosphonate, MeP(O)(F)(OH), (MF) (0.024 g, 0.241 mmol) in benzene was added dropwise that induced a color change from red to yellow. Volatiles were then removed from the reaction solution, and the residue was dissolved in ∼2 mL of hexane. The solution was allowed to sit undisturbed at room temperature, and over the course of 16 h, small clusters of X-ray diffraction quality orange needles formed. The orange crystalline material was isolated via decantation of the mother liquor and held under reduced pressure to a constant mass. Analysis of the material confirmed formation of 7 (0.078 g, 63%). Note: The benzene solution of MF is kept as a solid at −30 °C. At room temperature, MF will slowly enter an equilibrium with methylphosphonic acid (MPA) and difluoromethylphosphonate (DF). ^{31}P NMR analysis of MF is encouraged before use. Anal. calcd for $C_{19}H_{40}FMnNO_4P_3$: C, 44.45; H, 7.85; N, 2.73. Found: C, 44.61; H, 7.84; N, 2.74. ^{1}H NMR (C_6D_6, 20 °C): δ 5.73 (t, J = 11.9 Hz, 1H, N−H), 2.85 (m, 3H), 2.37 (h, J = 7.4 Hz, 1H), 2.30−1.90 (m, 5H), 1.79 (q, J = 14.0 Hz, 3H), 1.49 (ddd, J = 23.9, 14.5, 7.5 Hz, 6H), 1.39−1.15 (m, 15H), 1.08 (t, J = 8.4 Hz, 3H), 1.00 (t, J = 8.0 Hz, 3H). ^{31}P{^{1}H} NMR (C_6D_6, 20 °C): δ 84.45−83.74 (q), 36.97−31.01 (d, J = 965 Hz). ^{19}F NMR (C_6D_6, 20 °C): δ −43.59, −46.15 (d, J = 965 Hz). ^{13}C{^{1}H} NMR (C_6D_6, 20 °C): δ 230.9, 229.6, 53.2−52.4 (dq), 27.5 (t), 25.7−25.6 (dd), 24.5−24.2 (dd), 20.5, 20.1, 18.9−18.9 (d), 18.0−17.6 (dd), 14.2−12.3 (dd).

Synthesis and Characterization

Mn−F Synthesis. The stoichiometric generation of H−F resulting from the hydrolysis of P−F bonds remains a noteworthy complication to address for catalytic degradation of organophosphorus CWAs. Farha has built a polymeric amine into his MOF catalysts as a means of addressing H−F generation.[64] Here, the hydrolysis of P−F bonds is expected to generate HF and the corresponding P−OH, both of which are anticipated to react with (^{iPr}PNP)Mn(CO)$_2$ (**1**). Initial efforts were concentrated on synthesizing and characterizing the expected products from exposure of (^{iPr}PN^{H}P)Mn(CO)$_2$(OH) (**2**) to a P−F compound. The corresponding manganese phosphate adduct would form concomitant with generation of HF, which in turn would generate (^{iPr}PN^{H}P)Mn(CO)$_2$F (**3**) (Scheme 1). The expected Mn−F product has yet to be reported, and its synthesis was pursued to help identify this expected product in reactions of fluorophosphate substrates.

Independent generation of **3** was achieved *via* salt metathesis of silver fluoride with (^{iPr}PN^{H}P)Mn(CO)$_2$Br (**1-Br**). Complex **3** was

https://doi.org/10.1021/acsorginorgau.3c00003
ACS Org. Inorg. Au 2023, 3, 199−208

isolated as a yellow crystalline material in moderate yields. NMR experiments suggest the product of halogen exchange formed, with the ^{1}H and ^{31}P spectra reminiscent of **1-Br** but with a resonance in the ^{19}F NMR spectrum centered at δ −378.63 ppm. Unambiguous assignment of the structure of **3** was accomplished through single-crystal X-ray diffraction (SC-XRD) experiments (Figure 2). Complex

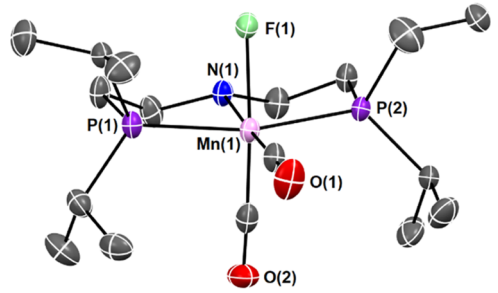

Figure 2. Solid-state structure of **3** is provided and represented at 50% probability ellipsoids. Hydrogen atoms have been removed for clarity.

3 crystallizes with two molecules in the asymmetric unit in the $P2\bar{1}n$ space group. The geometry of **3** closely resembles previously reported ($^{iPr}PN^{H}P$)Mn(CO)$_2$(X) complexes.[55] The Mn−F bond was found at 2.009(1) Å, slightly shorter than the Mn−O bond in **2**, which averages 2.070(2) Å. This Mn−F bond length is in line with a previously reported Mn(I) terminal fluoride.[65] The largest deviation from an ideal octahedral comes from apparent hydrogen bonding between the N−H proton and F atom, leading to an average N−Mn−F bond angle of 78.75°. This acute bond leads to a much shorter F−N distance (at 2.673(1) Å) than the observed O−N length in **2** (2.803(2) Å).

1,2-Addition Reactivity. To synthesize the expected manganese−phosphate and −phosphonate complexes, the well-established 1,2-addition chemistry of phosphorus acid substrates to complex **1** was employed (Scheme 2). The small-molecule diisopropylphosphate (DIP) displays a similar steric profile as diisopropylfluorophosphate (DIFP), commonly employed as a surrogate molecule for G-agents, such as sarin. Addition of DIP to **1** did not result in an observable reaction. Addition of one equivalent of H_2O to a solution containing an equimolar mix of **1** and DIP induced a color change from red to yellow. Formation of complex ($^{iPr}PN^{H}P$)Mn(CO)$_2$(OP(O)(O^{i}Pr)$_2$) (**4**) required the addition of H_2O, likely forming a complex hydrogen network between the Mn(I) center and the two substrates that facilitates the 1,2-addition. Analysis of the reaction by ^{31}P NMR indicated complete conversion to **4**. Complex **4** was stable to 1,2-elimination once formed, with no generation of **1** observed upon raising the solution temperature as determined using VT NMR experiments.

Confirmation of the formation of **4** was accomplished by performing SC-XRD studies; the solid-state structure was determined by isolating small yellow needles from a concentrated benzene solution (Figure 3, left). Complex **4** crystallizes in the $P\bar{1}$ space group with a single molecule of benzene in the lattice. The Mn−O bond length of complex **4** was found at 2.080(1) Å, and the two terminal P−O bond lengths, P−O3 = 1.497(1) Å and P−O4 = 1.482(1) Å, suggest resonance delocalization of the negative charge across the two oxygen atoms. There is observed hydrogen bonding between the N−H and O4 of the phosphate fragment, leading to a N1−O4 distance of 3.071(2) Å and a O4−H1 (calculated) distance of 2.156(1) Å. In the ^{1}H NMR, this translates to a N−H triplet centered at δ 5.43 ppm, suggesting weak H-bonding interactions when compared to the hydrogen bond found in the related formate complex (δ 8.18 ppm).[54] In the ^{31}P NMR spectrum, the PNP shifts are located at δ 84.18 ppm, and the bound phosphate signal is located at δ 4.57 ppm.

Scheme 2. 1,2-Addition Reactions between 1 and DIP (a), DMP (b), and MIP (c) Are Shown with the Corresponding Products

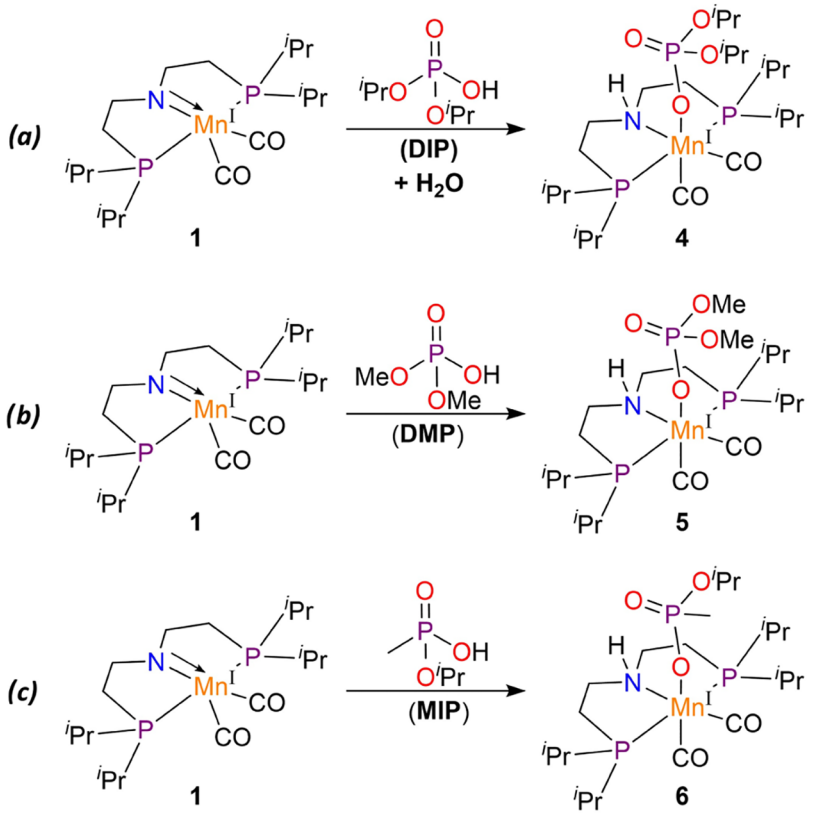

https://doi.org/10.1021/acsorginorgau.3c00003
ACS Org. Inorg. Au 2023, 3, 199−208

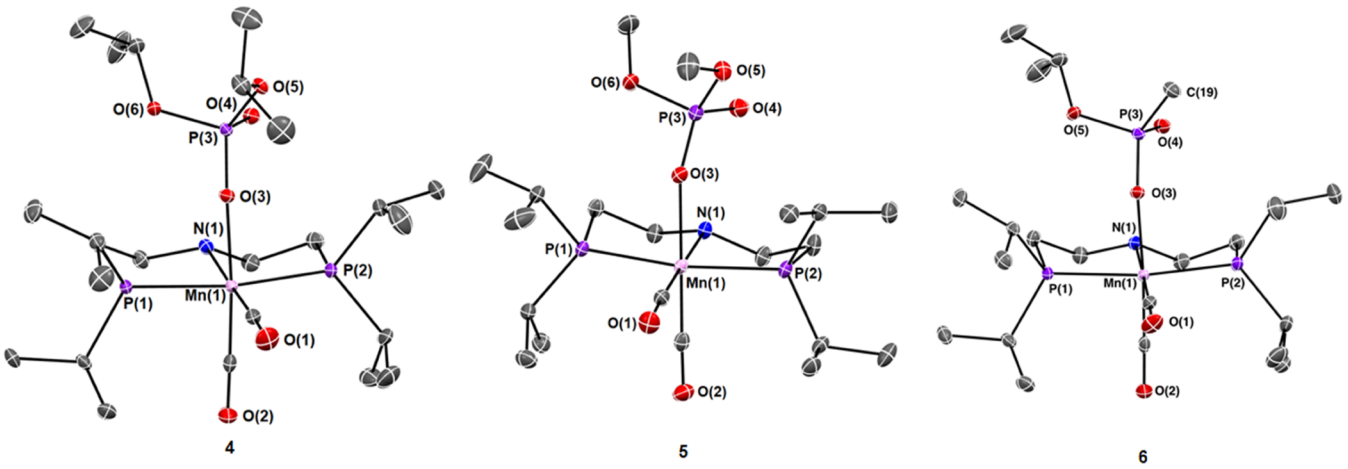

Figure 3. Solid-state structures of complexes **4**, **5**, and **6** are presented at 50% probability ellipsoids. Hydrogen atoms are omitted for clarity.

The prerequisite of water in the formation of **4** was likely due to kinetic inhibition arising from the steric demands of both the substrate and PNP ligand. Testing this hypothesis required a 1,2-addition reaction using a less sterically demanding phosphate, thus the reaction was performed with dimethylphosphate (DMP). Addition of DMP to a solution of **1** rapidly generated the expected (^{iPr}PN^{H}P)-Mn(CO)$_2$(OP(O)(OMe)$_2$) (**5**, Scheme 2b), and the expected color change of the solution from red to yellow upon substrate addition was observed. Without the sterically demanding isopropyl groups, the addition of the O−H bond across the Mn−amide bond readily occurs.

Complex **5** was isolated as a yellow crystalline material and the structure was confirmed by SC-XRD experiments (Figure 3, mid). The Mn−O bond length is consistent with those previously observed, at 2.110(1) Å. Like **4**, the phosphate fragment shows P−O terminal bonds of similar length, P−O3 = 1.499(1) Å and P−O4 = 1.483(1) Å. The phosphate geometry on **5** compared to **4** affords a slightly stronger hydrogen-bonding interaction with the N−H proton, with a measured N1−O4 distance of 2.918(1) Å and an O4−H1 distance of 1.945(1) Å. The ^{1}H NMR confirms this, with **5** showing a slightly more downfield N−H proton shift centered at δ 5.87 ppm. This is a result of the larger isopropyl groups on **4** causing more twist along the Mn−N1−O4−O3 plane leading to a longer interaction between H1 and O4.

The addition of methyl(isopropyl)phosphate (MIP) to **1** to generate (^{iPr}PN^{H}P)Mn(CO)$_2$(OP(O)Me(O^{i}Pr)) (**6**) was performed analogously to **5**. Complex **6** was isolated as yellow crystals and refinement of SC-XRD data revealed that **6** crystallized in the achiral space group $\bar{P}1$ and contained both enantiomers (*R*, *S*) of the Mn−phosphate in the unit cell (Figure 3, right). The phosphate oxygen atom O4 shows a hydrogen-bond distance of 2.095(2) Å to the N−H proton, while the corresponding P3−O4 bond was observed at 1.496(1) Å. The similarity of hydrogen-bond distance correlates with the ^{1}H NMR spectrum, where the triplet for the N1−H proton is found at δ 6.09 ppm, a shift consistent with slightly stronger hydrogen bonding than observed for **4** and **5**. Along with the N−H resonance, **6** has several diagnostic features observable in its NMR spectra. The PNP−chelate phosphorus resonances are found at δ 84.53 ppm and the Mn-bound phosphate at δ 31.79 ppm with integration values of 2:1. The methyl bound to the phosphonate in **6** is found as a doublet (J_{P-C} = 139 Hz) in the ^{13}C NMR spectrum centered at δ 14.3 ppm, shifted from free MIP (δ 11.98 ppm, J_{P-C} = 148 Hz).

MIP is related to sarin in its structure, with the −F of sarin replaced with an $^{-}$OH functionality. The 1,2-addition of MIP to **1** did not display kinetic impedance, yet DIFP is often employed as a surrogate for sarin, and the hydrolysis product DIP exhibited a kinetic barrier that is absent in the reactivity of MIP. This result highlights the drawback of employing a surrogate in CWA studies, as oftentimes surrogates fail to accurately reproduce the chemistry of live agents. In this case, the slow product formation upon addition of DIP to **1** is far removed from the rapidity of MIP addition. Formation of complex **6** from addition of MIP to **2** is analogous to the reaction between **2** and an aged G-agent that would be found on the serine residue of an AChE active site. As proof of concept for reactivity with an aged OPA, a reaction of **2** with the deprotonated phosphate of DIP was performed. A solution of DIP in THF was deprotonated with sodium hexamethyldisilazide (NaHMDS). The in situ-generated precipitate was then added to a C_6D_6 solution of **2**. Analysis of the solution by ^{31}P NMR confirmed rapid generation of **4**. This proof of concept further confirms the electrophilic nature of the PNP−Mn moiety that could react with an aged, anionic OPA.

The final Mn complex synthesized was the possible adduct that would form from the hydration reaction of **2** with methylphosphonic acid difluoride (difluor, DF). DF is a common precursor to organophosphorus CWAs, and its primary hydrolysis product is methylfluorophosphonic acid (monofluor, MF). The spectroscopic signatures and reactivity of MF are not well studied, and the manganese adducts of this unique organophosphate are germane to OPA degradation studies. The addition of MF to **1** generated the desired Mn-fluorophosphonate, (^{iPr}PN^{H}P)Mn(CO)$_2$(OP(O)MeF) (**7**), isolated in moderate yield as dark yellow crystalline blocks. Confirmation of the formation of **7** was achieved using NMR and IR spectroscopy and SC-XRD (Figure 4).

Complex **7** adopted a distorted octahedral geometry in the solid-state structure. Significant rotational disorder was present on the Mn-bound fluorophosphate, a consequence of the low steric profile of the substrate. The ^{1}H NMR spectrum was consistent with a phosphate bound to the [(^{iPr}PN^{H}P)Mn(CO)$_2$] core. The N−H resonance was

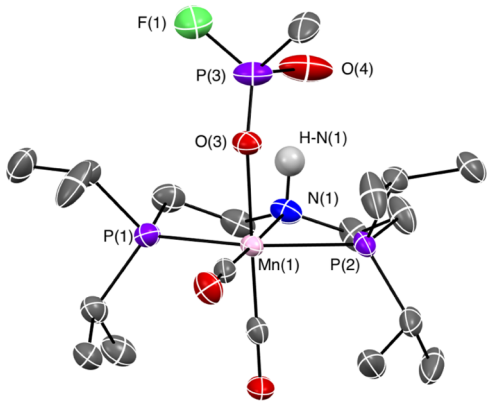

Figure 4. Solid-state structure of **7** represented at 50% probability ellipsoids. Disorder and hydrogen atoms have been omitted for clarity.

https://doi.org/10.1021/acsorginorgau.3c00003
ACS Org. Inorg. Au 2023, 3, 199−208

found as a triplet centered at δ 5.72 ppm by ^{1}H NMR, and the phosphate peak was found as a doublet centered at δ 33.99 (J_{P-F} = 965 Hz) by ^{31}P NMR. The large coupling constant is consistent with a P−F bond. The related resonance in the ^{19}F NMR spectrum was found as a doublet centered at δ −44.88 (J_{P-F} = 965 Hz). These shifts are similar to the spectrum of MF in C_6D_6.[58]

Complex **1** displayed productive reactivity with both neutral P−OH moieties and an anionic P−O$^-$ substrate. This breadth of [(^{iPr}PNP)Mn(CO)$_2$]-coordinated phosphate molecules (Table 1) provides a foundation to study similar reactivity with live agents.

Table 1. Select Metrical Parameters of the Complexes Generated or Used in This Study[a]

	^{1}H N−H[b]	^{31}P PNP[b]	^{31}P OPA[b]	ν CO IR[c]
1[54]		87.02		1800, 1888
3		89.16		1801, 1896
4	5.43	84.18	4.57	1811, 1918
5	5.87	84.30	9.30	1810, 1906
6	6.09	84.53	31.79	1814, 1911
7	5.73	84.45−83.74	33.99	1817, 1912

[a]Further tabular data can be found on Page S36. [b]Data given in ppm (δ). [c]Data given in cm^{-1}.

Nucleophilic Mn−OH Reaction with DIFP. Complexes of (^{iPr}PN^{H}P)Mn(CO)$_2$(X) derived from the hydration of **2** with electrophiles have shown little propensity for turnover without forcing conditions such as high temperatures (>100 °C) or the addition of strong bases.[43−56] Experiments into the reactivity and turnover of **2** with DIFP yielded mixed results. Complex **2** crystallizes with three molecules of water in the unit cell, so reactions can be expected to contain excess H_2O. When the reaction is performed in a 1:1 ratio of **2** to DIFP, half of the starting DIFP remains unreacted, and the Mn was found as an equimolar mixture of **3** and **4** as predicted (Scheme 1). Addition of 2 equivalents of **2** to 1 equiv of DIFP in C_6D_6 completely consumes the DIFP to form a 1:1 ratio of **3** and **4**, confirmed by ^{31}P and ^{19}F NMR (Figures S23−25). Complex **3** arises from the formation of H−F upon the hydrolysis of the P−F bond of DIFP. These results suggest that the rate of addition of H−F is faster than addition of DIFP, an unsurprising result given the steric demand of the DIFP substrate.

Absence of phosphate release from **4** was verified by employing 2 equiv of DIFP, where the extra equivalent of substrate remained unconsumed and the final reaction ratio of **4** to **DIFP** was found at approximately 1:1 using ^{31}P NMR spectroscopy. The addition of excess H_2O to encourage substrate release from **4** also proved unsuccessful due to overwhelming product inhibition of the catalyst. Addition of triethylamine (TEA) and 1,4-diazabicyclo[2.2.2]octane (DABCO) both proved ineffective for either phosphate or fluoride release. Employing K_2CO_3 as a base during the reaction resulted in conversion of **3** into **2**, which was then converted further into **4** with remaining DIFP (Figures S25 and S26). This suggests that the fluoride is more readily removed than the phosphate substrate, increasing the concentration of **4** in solution. The only reaction conditions that proved effective for phosphate release were found by employing a strong base; the addition of potassium bis(trimethylsilyl)amide (KHMDS) proved effective for substrate release as the potassium phosphate with concomitant generation of **1** (Figures S27 and S28).

^{17}OH$_2$ Labeling Studies. In two cases of phosphate addition to the Mn center, either the addition of bulky DIP with H_2O facilitating the addition or the nucleophilic reaction of **2** to DIFP, water plays a pivotal role. To better understand the role of water in these systems, a series of labeling studies were performed using ^{17}OH$_2$ (^{17}O, I = 1/2 nucleus). In this way, we were able to compare the incorporation of the labeled atom in two distinct reactions where **4** is a common product. During the 1,2-addition of DIP in the generation of **4**, does water act as a simple proton shuttle or does the ^{17}O incorporate into the phosphate? Is incorporation of ^{17}O observed in the reaction between **^{17}OH-2** and DIFP? Water is expected to form complex hydrogen-bond networks in this system,[55,66] complicating the answers to these questions, but labeling the ^{17}O may prove informative.

Control experiments designed to study potential ^{17}O exchange were performed with DIP and ^{17}OH$_2$, and no incorporation of ^{17}O signal was observed in DIP. However, exchange into DIP does occur in the presence of **2**. Complex **2** was ^{17}O labeled by addition of ^{17}OH$_2$ to **1**, giving **^{17}O-2**, which likely contains the same excess water molecules in the unit cell as natural abundance of **2**. The signal for the Mn−^{17}OH appears in the ^{17}O NMR spectrum at δ −109 ppm (referenced to ^{17}OH$_2$, Figure S30). When DIP is added to the **^{17}O-2**, the color of the solution changes from red to yellow, and new ^{17}O signals are immediately apparent as a broad singlet at δ 105 ppm and a doublet (J = 353 Hz) centered at δ 386 ppm (Figures S31 and S32). The resonance at 105 ppm is attributed to the Mn−O−P bridging atom, while the doublet at δ 386 ppm is assigned as the P═O double bond, with support from prior reports of ^{17}O-labeled DIP.[67] After 1 h, the signal for **2** is consumed and the resonances at δ 105 ppm and δ 386 ppm remain.

We propose that the tandem incorporation of ^{17}O into the two available positions of DIP (Scheme 3) may speak to an outer-sphere mechanism, where DIP$^-$ is formed and this ionic phosphate then incorporates ^{17}O via exchange with labeled water before Mn coordination. An outer-sphere mechanism may explain the observed ^{17}O product with incorporation in both sites in **^{17}O-4**. While NMR experiments showed lack of observable reversibility of **4** at elevated temperatures in solution, an equilibrium could exist that allows for rapid dissociation and label incorporation into the phosphate before recombination with the Mn center, which could occur faster than the NMR timescale. Both instances generate a common DIP$^-$ intermediate (Figure S41).

Scheme 3. Incorporation of ^{17}O-Labeled Water Into Both Possible Positions of ^{17}O-4 Was Observed During the Reaction of ^{17}O-2 with DIP

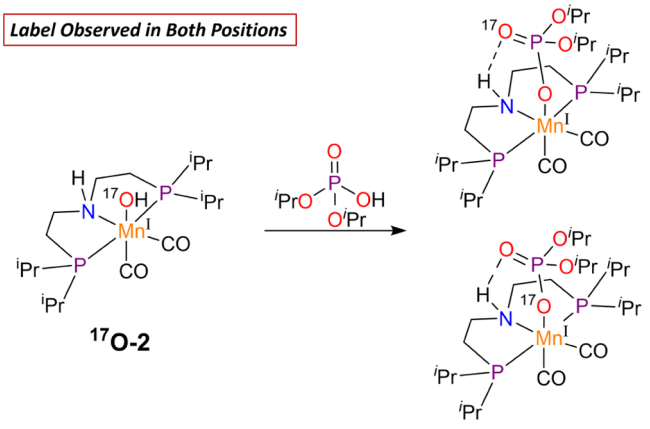

After 4 days, the doublet at δ 386 ppm increases, with only a trace signal at δ 105 ppm remaining. This leads to the hypothesis that the ^{17}O is preferred in the terminal P═O position, bearing a hydrogen bond to the N−H proton. Complete consumption of the ^{17}OH$_2$ signal and growth of a second small doublet at δ 377 ppm (J = 393 Hz) and singlet at δ 96 ppm were observed. Interconversion of the oxygen atoms is reasonable as the two terminal P−O oxygen atoms plausibly exchange positions, but the heavy isotope of the O atom preferentially occupies the hydrogen-bound position.

The addition of DIFP to **^{17}O-2** was expected to cleave the P−F bond and form **3** and **4** in equal parts, with the ^{17}O atom thus forming the Mn−O−P bridge atom (Scheme 4). Control experiments showed that no reaction occurred between **^{17}O-2** and DIFP over the course of 2 weeks. The reaction was performed with different equivalents of **^{17}O-2−DIFP**, either using substoichiometric Mn in a ratio of 0.33:1

https://doi.org/10.1021/acsorginorgau.3c00003
ACS Org. Inorg. Au 2023, 3, 199−208

Scheme 4. Incorporation of ^{17}O-Labeled Water into a Single Position of the Phosphate in 4 Is Observed Rather than as a Distribution

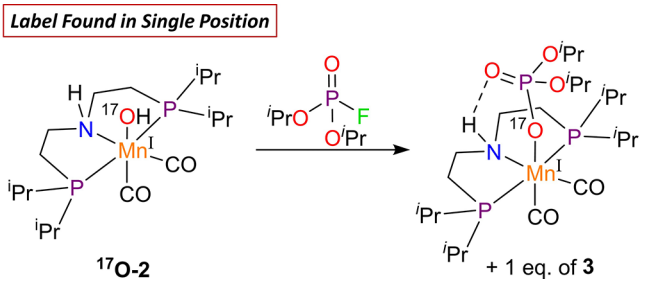

of ^{17}**O-2−DIFP**, or performing the stoichiometric reaction 1:1 ^{17}**O-2−DIFP**. In both cases, the ^{17}O NMR experiments reveal that the label incorporation occurs at the Mn−O−P position. For the 1:1 reaction, the ^{17}O begins to equilibrate between the two positions after time. However, when performed with substoichiometric quantities of ^{17}**O-2**, the ^{17}O resonance was stable in the Mn−O−P position and showed minimal incorporation into the P═O position after extended periods of time (Figure S42). These results are distinct from the observation of ^{17}**O-2** and DIP, where resonances attributed to both positions arise simultaneously. Additionally, secondary products arising from decomposition were not observed. The absence of excess $^{17}OH_2$ limits the subsequent exchange that occurs and the ^{17}O label remains in a single position in the molecule. Prior studies exploring nitrile hydration catalysis with **2** describe outer-sphere hydroxide as the lower-energy pathway for the nucleophilic attack on the nitrile as opposed to [Mn−OH].[68] An outer-sphere mechanism could be expected to produce the Mn−phosphate product with a distribution of ^{17}O incorporation into the P═O double bond and Mn−O−P bridging atom (Figure S42), a product distribution which was not observed.

Following extended reaction times, the reaction solutions containing ^{17}**O-4** in the presence of excess labeled water begin to show signs of decomposition with the appearance of a new doublet at δ 377 ppm, as well as a broadened singlet at δ 96 ppm (Scheme 5).

Scheme 5. Observed Reaction of 4 Generating the Decomposition Product 8

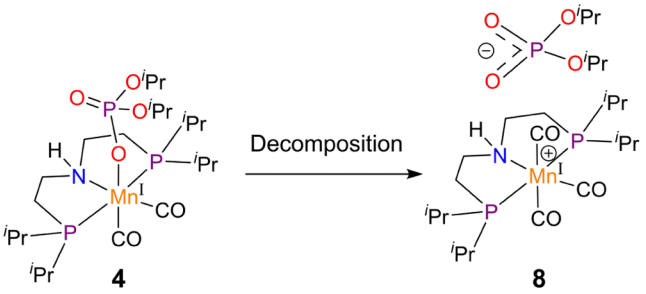

This additional species is shifted ∼10 ppm from the resonances of ^{17}**O-4** and is derived from decomposition of ^{17}**O-4**. The NMR tube solutions of the reactions were held under reduced pressure to remove volatiles, and the syrupy orange residue was taken into hexane and allowed to sit undisturbed at room temperature, whereupon two morphologies of crystals formed: orange blocks and pale yellow plates (Figure S43). The crystals were physically separated and analyzed with NMR and IR spectroscopies and SC-XRD analysis, which confirmed the orange blocks as ^{17}**O-4** (Figure S44). Further characterization of the material was hampered due to impurities and excess water from the reaction mixture, but the results of the NMR were informative. The ^{17}O NMR spectrum confirmed the previous assignments of ^{17}**O-4** as the resonances at δ 105 ppm and δ 386 ppm (Figure S45a). The ATR IR spectra of **4** and ^{17}**O-4** were compared to find a difference in stretches due to the presence of ^{17}O but were unsuccessful.

The pale yellow crystals were analyzed using NMR and IR spectroscopies and SC-XRD analysis. The ^{1}H spectrum was not informative when performed in C_6D_6 at room temperature, with the spectrum consisting of only broadened, nondescript resonances. The ^{31}P NMR spectrum was also broad, but the observed peaks at δ 93.3 ppm and δ 0.0 ppm are consistent with the presence of [^{iPr}PNPMn] and phosphate fragments. Analysis of the ^{17}O NMR spectrum, however, confirmed that this material gave rise to the ingrowth of resonances at δ 377 ppm and δ 96 ppm (Figure S47c). Determination of the identity of the material was accomplished through SC-XRD experiments. A model of $[(^{iPr}PN^{H}P)Mn(CO)_3][PO_2(O^iPr)_2]$ (**8**, Figure S48) was found and assigned to the material. The slight shift of the ^{17}O resonances is consistent with a complex resembling ^{17}**O-4**.

The results of the ^{17}O labeling experiments helped further characterize the complexes **2** and **4**, as well as provided insight into the role of water in two separate reactions that produce the same product. During the formation of ^{17}**O-4** via the addition of DIP to ^{17}**O-2**, an outer-sphere $[PO_2(O^iPr)_2]^-$ ion is likely present that can exchange with $^{17}OH_2$ before coordination to $[(^{iPr}PN^{H}P)Mn(CO)_2]^+$. The cleavage of the P−F bond of DIFP using ^{17}**O-2** did not show evidence of the expected product distribution of an outer-sphere mechanism. The ^{17}O label was found in the Mn−O−P position, followed by slow scrambling into the P═O bond in the presence of excess $^{17}OH_2$. Additional information on the decomposition of ^{17}**O-4** was found due to labeling experiments, leading to the identification of **8**. The broad featureless resonances of **8** were not evident in the reactions of natural abundance, yet the ^{17}O NMR spectrum distinctly showed an additional product forming over time, with an ∼10 ppm downfield shift. A summary of assigned ^{17}O NMR shifts is provided (Table 2).

Table 2. Assigned ^{17}O NMR Shifts[a] of Labeled Complexes Observed in These Studies

	^{17}O-2	^{17}O-4	8
Mn-^{17}OH	−110		
P═^{17}O		386 (353 Hz)	377 (393 Hz)
P-^{17}O-Mn		107	96

[a]Reported in ppm with observed coupling (Hz).

SUMMARY AND CONCLUSIONS

This study focusing on small-molecule organophosphates was performed to highlight the ambiphilic behavior of **1**, a property that may show utility for ameliorating the effects of organophosphate exposure. The manganese center was shown to interact with several small-molecule phosphorus compounds, either with or without the presence of water. The electrophilic complex **1** was competent for phosphate binding through 1,2-addition reactivity of the O−H bond for several distinct small-molecule OPAs. For the most sterically demanding substrate, DIP, the addition of water was necessary for the conversion to **4**. Importantly, **2** also binds anionic phosphate, drawing a comparison of functional groups present in an aged complex of OPA in the binding site of AchE.

The nucleophilic manganese hydroxide complex **2** was shown to facilitate the cleavage of the P−F bond of DIFP and form the corresponding phosphate complex **4** with concomitant formation of **3**. Amine bases were ineffective for substrate release. Employing K_2CO_3 in the presence of excess DIFP resulted in the consumption of **3** and further generation of **4**. These results indicated a stronger phosphate bond to Mn, with fluoride more easily displaced. Release of the phosphate

https://doi.org/10.1021/acsorginorgau.3c00003
ACS Org. Inorg. Au 2023, 3, 199−208

fragment from **4** was only achieved by employing highly basic KHMDS.

Labeling reactions were performed to explore potential mechanisms in the formation of ^{17}**O-4**. The simple addition of DIP to **1** does not proceed without the addition of water. Performing this reaction with ^{17}**O-2** gave a product where the ^{17}O label is present in both oxygen atoms of the phosphate in near equal ratios. Contrast this to the results of the addition of ^{17}**O-2** to DIFP, where the ^{17}O label is observed in the Mn−O−P bridge atom as the initial product, followed by slow scrambling into the P═O position in the presence of excess $^{17}OH_2$. Further studies are necessary to provide stronger mechanistic evidence, but these results suggest different processes based on positional label incorporation of the resultant Mn−phosphate.

This set of experiments provides evidence for the reactivity between electrophilic metal [^{iPr}PNPMn] complexes—and nucleophilic [^{iPr}PNPMn-OH] derivatives—and small-molecule organophosphorus complexes related to CWAs. Further investigation of transition-metal catalysts bearing similar ambiphilic properties may provide a complementary toolbox to address CWA exposure and the amelioration of its effects. We will continue to pursue electrophilic metal complexes as an entry point to activate and pacify phosphorus compounds in both pre- and postexposure conditions.

■ ASSOCIATED CONTENT

Data Availability Statement

The data underlying this study are available in the published article and its Supporting Information.

Supporting Information

The Supporting Information is available free of charge at https://pubs.acs.org/doi/10.1021/acsorginorgau.3c00003.

Additional experimental procedures, spectra, crystallographic tables, and CCDC deposition numbers for complexes **3**−**8** are provided (PDF).

Deposition numbers for the CCDC of 2212320−2212326 contain the supplementary crystallographic data for this paper. These data can be obtained free of charge via www.ccdc.cam.ac.uk/data_request/cif, or by emailing data_request@ccdc.cam.ac.uk, or by contacting The Cambridge Crystallographic Data Center, 12 Union Road, Cambridge CB2 1EZ, UK; fax: +44 1223 336033.

Accession Codes

CCDC 2212320−2212326 contain the supplementary crystallographic data for this paper. These data can be obtained free of charge via www.ccdc.cam.ac.uk/data_request/cif, or by emailing data_request@ccdc.cam.ac.uk, or by contacting The Cambridge Crystallographic Data Centre, 12 Union Road, Cambridge CB2 1EZ, UK; fax: +44 1223 336033.

■ AUTHOR INFORMATION

Corresponding Authors

Brennan S. Billow − *Los Alamos National Laboratory, Los Alamos, New Mexico 87544, United States;* orcid.org/0000-0002-7560-9369; Email: billowbr@lanl.gov

Aaron M. Tondreau − *Los Alamos National Laboratory, Los Alamos, New Mexico 87544, United States;* orcid.org/0000-0003-0440-5497; Email: tondreau_a@lanl.gov

Authors

Brooke N. Livesay − *Los Alamos National Laboratory, Los Alamos, New Mexico 87544, United States;* orcid.org/0000-0002-8549-9458

Jurgen G. Schmidt − *Los Alamos National Laboratory, Los Alamos, New Mexico 87544, United States*

Robert F. Williams − *Los Alamos National Laboratory, Los Alamos, New Mexico 87544, United States;* orcid.org/0000-0002-4310-6249

Complete contact information is available at: https://pubs.acs.org/10.1021/acsorginorgau.3c00003

Notes

The authors declare no competing financial interest.

■ ACKNOWLEDGMENTS

This work was conceived and executed at Los Alamos National Laboratory. Los Alamos National Laboratory is operated by Triad National Security, LLC, for the National Nuclear Security Administration of U.S. Department of Energy (Contract No. 89233218CNA000001). A.M.T. acknowledges Director's funded postdoctoral fellowship from Los Alamos National Laboratory for support, with special recognition of Science Campaign 5 for support of the development of a suite of catalysts, including complexes **1** and **2**. The $^{17}OH_2$ labeling studies were supported by the U.S. Department of Energy, Office of Science, Office of Basic Energy Sciences, Heavy Element Chemistry program under Award Number 2020LANLE372. A.M.T. also thank Sarah K. Tondreau for assistance with manuscript organization and copyediting. Brennan Billow acknowledges both an Agnew National Security Fellowship and an LDRD Early Career Award (20220540ECR) for partial support of this work.

■ REFERENCES

(1) Munro, N. Toxicity of the Organophosphate Chemical Warfare Agents GA, GB, and VX: Implications for Public Protection. *Environ. Health Perspect.* **1994**, *102*, 18−37.

(2) Weetman, C.; Notman, S.; Arnold, P. L. Destruction of Chemical Warfare Agent Simulants by Air and Moisture Stable Metal NHC Complexes. *Dalton Trans.* **2018**, *47*, 2568−2574.

(3) Courtney, R. C.; Gustafson, R. L.; Westerback, S. J.; Hyytiainen, H.; Chaberek, S. C.; Martell, A. E. Metal Chelate Compounds as Catalysts in the Hydrolysis of Isopropyl Methylphosphonofluoridate and Diisopropylphosphorofluoridate 1. *J. Am. Chem. Soc.* **1957**, *79*, 3030−3036.

(4) Ward, J. R.; Szafraniec, L. L.; Beaudry, W. T.; Hovanec, J. W. On the Mechanism of Phosphono or Phosphorofluoridate Hydrolysis Catalyzed by Transition Metal Ions. *J. Mol. Catal.* **1990**, *58*, 373−378.

(5) Hay, R. W.; Govan, N.; Parchment, K. E. A Metallomicelle Catalysed Hydrolysis of a Phosphate Triester, a Phosphonate Diester and O-Isopropyl Methylfluorophosphonate (Sarin). *Inorg. Chem. Commun.* **1998**, *1*, 228−231.

(6) Jabbour, C. R.; Parker, L. A.; Hutter, E. M.; Weckhuysen, B. M. Chemical Targets to Deactivate Biological and Chemical Toxins Using Surfaces and Fabrics. *Nat. Rev. Chem.* **2021**, *5*, 370−387.

(7) Johnson, E. M.; Boyanich, M. C.; Gibbons, B.; Sapienza, N. S.; Yang, X.; Karim, A. M.; Morris, J. R.; Troya, D.; Morris, A. J. Aqueous-Phase Destruction of Nerve-Agent Simulants at Copper Single Atoms in UiO-66. *Inorg. Chem.* **2022**, *61*, 8585−8591.

(8) Zammataro, A.; Santonocito, R.; Pappalardo, A.; Trusso Sfrazzetto, G. Catalytic Degradation of Nerve Agents. *Catalysts* **2020**, 881.

(9) McCarthy, D. L.; Liu, J.; Dwyer, D. B.; Troiano, J. L.; Boyer, S. M.; DeCoste, J. B.; Bernier, W. E.; Jones, W. E., Jr Electrospun Metal−Organic Framework Polymer Composites for the Catalytic Degradation of Methyl Paraoxon. *New J. Chem.* **2017**, *41*, 8748−8753.
(10) Lu, A. X.; McEntee, M.; Browe, M. A.; Hall, M. G.; DeCoste, J. B.; Peterson, G. W. MOFabric: Electrospun Nanofiber Mats from PVDF/UiO-66-NH_2 for Chemical Protection and Decontamination. *ACS Appl. Mater. Interfaces* **2017**, *9*, 13632−13636.
(11) Shen, C.; Mao, Z.; Xu, H.; Zhang, L.; Zhong, Y.; Wang, B.; Feng, X.; Tao, C.; Sui, X. Catalytic MOF-Loaded Cellulose Sponge for Rapid Degradation of Chemical Warfare Agents Simulant. *Carbohydr. Polym.* **2019**, *213*, 184−191.
(12) Kalaj, M.; Denny, M. S.; Bentz, K. C.; Palomba, J. M.; Cohen, S. M. Nylon−MOF Composites through Postsynthetic Polymerization. *Angew. Chem.* **2019**, *131*, 2358−2362.
(13) Jung, D.; Das, P.; Atilgan, A.; Li, P.; Hupp, J. T.; Islamoglu, T.; Kalow, J. A.; Farha, O. K. Reactive Porous Polymers for Detoxification of a Chemical Warfare Agent Simulant. *Chem. Mater.* **2020**, *32*, 9299−9306.
(14) Lee, D. T.; Zhao, J.; Peterson, G. W.; Parsons, G. N. Catalytic "MOF-Cloth" Formed via Directed Supramolecular Assembly of UiO-66-NH_2 Crystals on Atomic Layer Deposition-Coated Textiles for Rapid Degradation of Chemical Warfare Agent Simulants. *Chem. Mater.* **2017**, *29*, 4894−4903.
(15) Song, L.; Zhao, T.; Yang, D.; Wang, X.; Hao, X.; Liu, Y.; Zhang, S.; Yu, Z.-Z. Photothermal Graphene/UiO-66-NH2 Fabrics for Ultrafast Catalytic Degradation of Chemical Warfare Agent Simulants. *J. Hazard. Mater.* **2020**, *393*, No. 122332.
(16) Yao, A.; Jiao, X.; Chen, D.; Li, C. Bio-Inspired Polydopamine-Mediated Zr-MOF Fabrics for Solar Photothermal-Driven Instantaneous Detoxification of Chemical Warfare Agent Simulants. *ACS Appl. Mater. Interfaces* **2020**, *12*, 18437−18445.
(17) Ma, K.; Islamoglu, T.; Chen, Z.; Li, P.; Wasson, M. C.; Chen, Y.; Wang, Y.; Peterson, G. W.; Xin, J. H.; Farha, O. K. Scalable and Template-Free Aqueous Synthesis of Zirconium-Based Metal−Organic Framework Coating on Textile Fiber. *J. Am. Chem. Soc.* **2019**, *141*, 15626−15633.
(18) Chen, Z.; Ma, K.; Mahle, J. J.; Wang, H.; Syed, Z. H.; Atilgan, A.; Chen, Y.; Xin, J. H.; Islamoglu, T.; Peterson, G. W.; Farha, O. K. Integration of Metal−Organic Frameworks on Protective Layers for Destruction of Nerve Agents under Relevant Conditions. *J. Am. Chem. Soc.* **2019**, *141*, 20016−20021.
(19) Dwyer, D. B.; Dugan, N.; Hoffman, N.; Cooke, D. J.; Hall, M. G.; Tovar, T. M.; Bernier, W. E.; DeCoste, J.; Pomerantz, N. L.; Jones, W. E. Chemical Protective Textiles of UiO-66-Integrated PVDF Composite Fibers with Rapid Heterogeneous Decontamination of Toxic Organophosphates. *ACS Appl. Mater. Interfaces* **2018**, *10*, 34585−34591.
(20) Lu, A. X.; McEntee, M.; Browe, M. A.; Hall, M. G.; DeCoste, J. B.; Peterson, G. W. MOFabric: Electrospun Nanofiber Mats from PVDF/UiO-66-NH_2 for Chemical Protection and Decontamination. *ACS Appl. Mater. Interfaces* **2017**, *9*, 13632−13636.
(21) Zhao, J.; Lee, D. T.; Yaga, R. W.; Hall, M. G.; Barton, H. F.; Woodward, I. R.; Oldham, C. J.; Walls, H. J.; Peterson, G. W.; Parsons, G. N. Ultra-Fast Degradation of Chemical Warfare Agents Using MOF-Nanofiber Kebabs. *Angew. Chem.* **2016**, *128*, 13418−13422.
(22) Kalinovskyy, Y.; Wright, A. J.; Hiscock, J. R.; Watts, T. D.; Williams, R. L.; Cooper, N. J.; Main, M. J.; Holder, S. J.; Blight, B. A. Swell and Destroy: A Metal−Organic Framework-Containing Polymer Sponge That Immobilizes and Catalytically Degrades Nerve Agents. *ACS Appl. Mater. Interfaces* **2020**, *12*, 8634−8641.
(23) Jang, Y. J.; Kim, K.; Tsay, O. G.; Atwood, D. A.; Churchill, D. G. Update 1 of: Destruction and Detection of Chemical Warfare Agents. *Chem. Rev.* **2015**, *115*, PR1−PR76.
(24) Kim, K.; Tsay, O. G.; Atwood, D. A.; Churchill, D. G. Destruction and Detection of Chemical Warfare Agents. *Chem. Rev.* **2011**, *111*, 5345−5403.
(25) Bobbitt, N. S.; Mendonca, M. L.; Howarth, A. J.; Islamoglu, T.; Hupp, J. T.; Farha, O. K.; Snurr, R. Q. Metal−Organic Frameworks for the Removal of Toxic Industrial Chemicals and Chemical Warfare Agents. *Chem. Soc. Rev.* **2017**, *46*, 3357−3385.
(26) Yang, Y. C.; Baker, J. A.; Ward, J. R. Decontamination of Chemical Warfare Agents. *Chem. Rev.* **1992**, *92*, 1729−1743.
(27) Tsang, J. S.; Neverov, A. A.; Brown, R. S. Billion-Fold Acceleration of the Methanolysis of Paraoxon Promoted by La(OTf)$_3$ in Methanol. *J. Am. Chem. Soc.* **2003**, *125*, 7602−7607.
(28) Desloges, W.; Neverov, A. A.; Brown, R. S. Zn^{2+} -Catalyzed Methanolysis of Phosphate Triesters: A Process for Catalytic Degradation of the Organophosphorus Pesticides Paraoxon and Fenitrothion. *Inorg. Chem.* **2004**, *43*, 6752−6761.
(29) Liu, T.; Neverov, A. A.; Tsang, J. S.; Brown, R. S. Mechanistic Studies of La3+- and Zn2+-Catalyzed Methanolysis of Aryl Phosphate and Phosphorothioate Triesters. Development of Artificial Phosphotriesterase Systems. *Org. Biomol. Chem.* **2005**, *3*, 1525−1533.
(30) Melnychuk, S. A.; Neverov, A. A.; Brown, R. S. Catalytic Decomposition of Simulants for Chemical Warfare V Agents: Highly Efficient Catalysis of the Methanolysis of Phosphonothioate Esters. *Angew. Chem.* **2006**, *118*, 1799−1802.
(31) Mitra, A.; DePue, L. J.; Parkin, S.; Atwood, D. A. Five-Coordinate Aluminum Bromides: Synthesis, Structure, Cation Formation, and Cleavage of Phosphate Ester Bonds. *J. Am. Chem. Soc.* **2006**, *128*, 1147−1153.
(32) Mitra, A.; Atwood, D. A.; Struss, J.; Williams, D. J.; McKinney, B. J.; Creasy, W. R.; McGarvey, D. J.; Durst, H. D.; Fry, R. Group 13 Chelates in Nerve Gas Agent and Pesticide Dealkylation. *New J. Chem.* **2008**, *32*, 783−785.
(33) Kuo, L. Y.; Adint, T. T.; Akagi, A. E.; Zakharov, L. Degradation of a VX Analogue: First Organometallic Reagent To Promote Phosphonothioate Hydrolysis Through Selective P−S Bond Scission. *Organometallics* **2008**, *27*, 2560−2564.
(34) Kuo, L. Y.; Bentley, A. K.; Shari'ati, Y. A.; Smith, C. P. Phosphonothioate Hydrolysis Turnover by Cp_2MoCl_2 and Silver Nanoparticles. *Organometallics* **2012**, *31*, 5294−5301.
(35) Kuo, L. Y.; Smith, C. P.; Head, A. R.; Lichtenberger, D. L. Phosphonothioate Hydrolysis through Selective P-S Bond Scission by Molybdenum Metallocenes. *Main Group Chem.* **2010**, *9*, 283−295.
(36) Wilhelm, C. M.; Snider, T. H.; Babin, M. C.; Jett, D. A.; Platoff, G. E.; Yeung, D. T. A Comprehensive Evaluation of the Efficacy of Leading Oxime Therapies in Guinea Pigs Exposed to Organophosphorus Chemical Warfare Agents or Pesticides. *Toxicol. Appl. Pharmacol.* **2014**, *281*, 254−265.
(37) Worek, F.; Thiermann, H.; Szinicz, L.; Eyer, P. Kinetic Analysis of Interactions between Human Acetylcholinesterase, Structurally Different Organophosphorus Compounds and Oximes. *Biochem. Pharmacol.* **2004**, *68*, 2237−2248.
(38) Steinberg, G. M.; Lieske, C. N.; Boldt, R.; Goan, J. C.; Podall, H. E. Model Studies for the Reactivation of Aged Phosphonylated Acetylcholinesterase. Use of Alkylating Agents Containing Nucleophilic Groups. *J. Med. Chem.* **1970**, *13*, 435−446.
(39) Millard, C. B.; Kryger, G.; Ordentlich, A.; Greenblatt, H. M.; Harel, M.; Raves, M. L.; Segall, Y.; Barak, D.; Shafferman, A.; Silman, I.; Sussman, J. L. Crystal Structures of Aged Phosphonylated Acetylcholinesterase: Nerve Agent Reaction Products at the Atomic Level. *Biochemistry* **1999**, *38*, 7032−7039.
(40) Li, H.; Schopfer, L. M.; Nachon, F.; Froment, M.-T.; Masson, P.; Lockridge, O. Aging Pathways for Organophosphate-Inhibited Human Butyrylcholinesterase, Including Novel Pathways for Isomalathion, Resolved by Mass Spectrometry. *Toxicol. Sci.* **2007**, *100*, 136−145.
(41) Yoder, R. J.; Zhuang, Q.; Beck, J. M.; Franjesevic, A.; Blanton, T. G.; Sillart, S.; Secor, T.; Guerra, L.; Brown, J. D.; Reid, C.; McElroy, C. A.; Doğan Ekici, Ö.; Callam, C. S.; Hadad, C. M. Study of *Para* -Quinone Methide Precursors toward the Realkylation of Aged Acetylcholinesterase. *ACS Med. Chem. Lett.* **2017**, *8*, 622−627.
(42) Zhuang, Q.; Franjesevic, A. J.; Corrigan, T. S.; Coldren, W. H.; Dicken, R.; Sillart, S.; DeYong, A.; Yoshino, N.; Smith, J.; Fabry, S.;

https://doi.org/10.1021/acsorginorgau.3c00003
ACS Org. Inorg. Au 2023, 3, 199−208

Fitzpatrick, K.; Blanton, T. G.; Joseph, J.; Yoder, R. J.; McElroy, C. A.; Ekici, Ö. D.; Callam, C. S.; Hadad, C. M. Demonstration of In Vitro Resurrection of Aged Acetylcholinesterase after Exposure to Organophosphorus Chemical Nerve Agents. *J. Med. Chem.* **2018**, *61*, 7034−7042.
(43) Owen, A. E.; Preiss, A.; McLuskie, A.; Gao, C.; Peters, G.; Bühl, M.; Kumar, A. Manganese-Catalyzed Dehydrogenative Synthesis of Urea Derivatives and Polyureas. *ACS Catal.* **2022**, *12*, 6923−6933.
(44) Zhao, M.; Li, X.; Zhang, X.; Shao, Z. Efficient Synthesis of C3-Alkylated and Alkenylated Indoles via Manganese-Catalyzed Dehydrogenation. *Chem.- Asian J.* **2022**, *17*, No. e202200483.
(45) Shao, Z.; Yuan, S.; Li, Y.; Liu, Q. Using Methanol as a Formaldehyde Surrogate for Sustainable Synthesis of *N* -Heterocycles via Manganese-Catalyzed Dehydrogenative Cyclization. *Chin. J. Chem.* **2022**, *40*, 1137−1143.
(46) Elangovan, S.; Neumann, J.; Sortais, J.-B.; Junge, K.; Darcel, C.; Beller, M. Efficient and Selective N-Alkylation of Amines with Alcohols Catalysed by Manganese Pincer Complexes. *Nat. Commun.* **2016**, *7*, No. 12641.
(47) Peña-López, M.; Piehl, P.; Elangovan, S.; Neumann, H.; Beller, M. Manganese-Catalyzed Hydrogen-Autotransfer C−C Bond Formation: α-Alkylation of Ketones with Primary Alcohols. *Angew. Chem.* **2016**, *128*, 15191−15195.
(48) Andérez-Fernández, M.; Vogt, L. K.; Fischer, S.; Zhou, W.; Jiao, H.; Garbe, M.; Elangovan, S.; Junge, K.; Junge, H.; Ludwig, R.; Beller, M. A Stable Manganese Pincer Catalyst for the Selective Dehydrogenation of Methanol. *Angew. Chem.* **2017**, *129*, 574−577.
(49) Gausas, L.; Donslund, B. S.; Kristensen, S. K.; Skrydstrup, T. Evaluation of Manganese Catalysts for the Hydrogenative Deconstruction of Commercial and End-of-Life Polyurethane Samples. *ChemSusChem* **2022**, *15*, No. e202101705.
(50) Zubar, V.; Haedler, A. T.; Schütte, M.; Hashmi, A. S. K.; Schaub, T. Hydrogenative Depolymerization of Polyurethanes Catalyzed by a Manganese Pincer Complex. *ChemSusChem* **2022**, *15*, No. e202101606.
(51) Kaithal, A.; Werlé, C.; Leitner, W. Alcohol-Assisted Hydrogenation of Carbon Monoxide to Methanol Using Molecular Manganese Catalysts. *JACS Au* **2021**, *1*, 130−136.
(52) Elangovan, S.; Topf, C.; Fischer, S.; Jiao, H.; Spannenberg, A.; Baumann, W.; Ludwig, R.; Junge, K.; Beller, M. Selective Catalytic Hydrogenations of Nitriles, Ketones, and Aldehydes by Well-Defined Manganese Pincer Complexes. *J. Am. Chem. Soc.* **2016**, *138*, 8809−8814.
(53) Kumar, A.; Janes, T.; Espinosa-Jalapa, N. A.; Milstein, D. Manganese Catalyzed Hydrogenation of Organic Carbonates to Methanol and Alcohols. *Angew. Chem., Int. Ed.* **2018**, *57*, 12076−12080.
(54) Tondreau, A. M.; Boncella, J. M. 1,2-Addition of Formic or Oxalic Acid to $^{-}$ N{CH $_2$ CH $_2$ (PiPr $_2$)} $_2$ -Supported Mn(I) Dicarbonyl Complexes and the Manganese-Mediated Decomposition of Formic Acid. *Organometallics* **2016**, *35*, 2049−2052.
(55) Tondreau, A. M.; Michalczyk, R.; Boncella, J. M. Reversible 1,2-Addition of Water To Form a Nucleophilic Mn(I) Hydroxide Complex: A Thermodynamic and Reactivity Study. *Organometallics* **2017**, *36*, 4179−4183.
(56) Anderson, N. H.; Boncella, J. M.; Tondreau, A. M. Investigation of Nitrile Hydration Chemistry by Two Transition Metal Hydroxide Complexes: Mn−OH and Ni−OH Nitrile Insertion Chemistry. *Organometallics* **2018**, *37*, 4675−4684.
(57) Tondreau, A. M.; Boncella, J. M. The Synthesis of PNP-Supported Low-Spin Nitro Manganese(I) Carbonyl Complexes. *Polyhedron* **2016**, *116*, 96−104.
(58) Kaseman, D. C.; Malone, M. W.; Tondreau, A.; Espy, M. A.; Williams, R. F. Quantitation of Nuclear Magnetic Resonance Spectra at Earth's Magnetic Field. *Anal. Chem.* **2021**, *93*, 15349−15357.
(59) Sheldrick, G. M. *SADABS*; University of Gottingen: Germany, 2005.
(60) Sheldrick, G. M. *SHELXT* − Integrated Space-Group and Crystal-Structure Determination. *Acta Crystallogr., Sect. A: Found. Adv.* **2015**, *71*, 3−8.
(61) Sheldrick, G. M. Crystal Structure Refinement with *SHELXL*. *Acta Crystallogr., Sect. C: Struct. Chem.* **2015**, *71*, 3−8.
(62) Sheldrick, G. M. A Short History of *SHELX*. *Acta Crystallogr., Sect. A: Found. Crystallogr.* **2008**, *64*, 112−122.
(63) Dolomanov, O. V.; Bourhis, L. J.; Gildea, R. J.; Howard, J. A. K.; Puschmann, H. *OLEX2*: A Complete Structure Solution, Refinement and Analysis Program. *J. Appl. Crystallogr.* **2009**, *42*, 339−341.
(64) Chen, Z.; Ma, K.; Mahle, J. J.; Wang, H.; Syed, Z. H.; Atilgan, A.; Chen, Y.; Xin, J. H.; Islamoglu, T.; Peterson, G. W.; Farha, O. K. Integration of Metal−Organic Frameworks on Protective Layers for Destruction of Nerve Agents under Relevant Conditions. *J. Am. Chem. Soc.* **2019**, *141*, 20016−20021.
(65) Becker, T. M.; Bauer, J. A. K.; Bene, J. E. D.; Orchin, M. A Novel Dimanganese Complex Linked by an Unusually Strong Hydrogen Bond. X-Ray Structure of the Hydrogen-Bonded Complex and Ab Initio Calculations. *J. Organomet. Chem.* **2001**, *629*, 165−170.
(66) Prejanò, M.; Marino, T.; Rizzuto, C.; Madrid Madrid, J. C.; Russo, N.; Toscano, M. Reaction Mechanism of Low-Spin Iron(III)- and Cobalt(III)-Containing Nitrile Hydratases: A Quantum Mechanics Investigation. *Inorg. Chem.* **2017**, *56*, 13390−13400.
(67) Gerlt, J. A.; Demou, P. C.; Mehdi, S. Oxygen-17 NMR Spectral Properties of Simple Phosphate Esters and Adenine Nucleotides. *J. Am. Chem. Soc.* **1982**, *104*, 2848−2856.
(68) Prejanò, M.; Alberto, M. E.; Russo, N.; Marino, T. Hydration of Aromatic Nitriles Catalyzed by Mn-OH Complexes: A Rationalization from Quantum Chemical Investigations. *Organometallics* **2020**, *39*, 3352−3361.

https://doi.org/10.1021/acsorginorgau.3c00003
ACS Org. Inorg. Au 2023, 3, 199−208